PCCP

Computational and NMR study of quaternary ammonium ion conformations in solution

Victor B. Luzhkov,*[a] Fredrik Österberg,[a] Parag Acharya,[b] Jyoti Chattopadhyaya[b] and Johan Åqvist*[a]

[a] *Department of Cell and Molecular Biology, Uppsala University, BMC, Box 596, S-751 24, Uppsala, Sweden. E-mail: vluz@xray.bmc.uu.se and aqvist@xray.bmc.uu.se*
[b] *Department of Bioorganic Chemistry, Uppsala University, BMC, Box 581, S-751 23, Uppsala, Sweden*

Received 10th April 2002, Accepted 2nd August 2002
First published as an Advance Article on the web 29th August 2002

Conformations around C–N bonds at the quaternary centre in tetraalkylammonium ions in water solution are investigated. Structures of Me_4N^+, Et_4N^+, *n*-Pr_4N^+, *n*-Bu_4N^+, and *n*-Pe_4N^+ are calculated using quantum mechanical HF and DFT methods together with the PCM solvent model. Relative solvation free energies of tetraalkylammonium ions are further estimated from microscopic molecular dynamics free energy perturbation simulations using the Gromos-87 and Amber-95 force fields. The predicted free energy difference in solution between two stable conformations of Et_4N^+, D_{2d} and S_4, is 0.6–1.0 kcal mol^{-1} (in favour of D_{2d}), which is in quantitative agreement with the recent Raman spectroscopy results. The energies of the g^+g^- conformations of Et_4N^+ are 3.6–4.0 kcal mol^{-1} higher. The ions with longer hydrocarbon chains show quite similar energy gap between D_{2d} and S_4. The torsion barrier for a two-step interconversion between the D_{2d} and S_4 structures is 9.5 kcal mol^{-1} (HF/6-31G(d) calculations). The computational results are augmented by NMR measurements of the Et_4N^+–I^- salt in aqueous solution, which predict a symmetric structure of Et_4N^+ in water. However, the D_{2d} and S_4 conformers are not discernible due to presumably high similarity of chemical shifts. The calculated conformational energetics in solution together with previously observed D_{2d}, S_4 and high-energy g^+g^--type structures of Et_4N^+, *n*-Pr_4N^+, and *n*-Bu_4N^+ in the solid state indicate that the carbon chain conformations at the quaternary ammonium centre sensitively depend on the actual microenvironment.

1. Introduction

Tetraalkylammonium ions have broad applications in physical, organic and biological chemistry, where in many cases the complexes of these ions with other molecules are of particular interest. Considerable efforts have been devoted to studies of the structure, thermodynamics and solution properties of these compounds.[1–10] A general postulate is that conformations of hydrocarbon chains in tetra *n*-alkylammonium ions are controlled by quaternary centre. The observed conformational pattern is thus explained by steric intramolecular interactions between the carbon atoms in the second and more distant positions from the central nitrogen atom, in which case the avoidance of unfavourable g^+g^- interactions is important.[1,11] According to this criterion, Et_4N^+, as well as tetra-*N*-alkylammonium ions with longer hydrocarbon chains, can adopt either a quasi-planar conformation with D_{2d} symmetry or quasi-pyramidal conformation with S_4 symmetry (Fig. 1). Intermolecular interactions of tetraalkylammonium ions are determined by both the total positive charge of +1 and by the nonpolar hydrocarbon groups which makes these compounds classical hydrophobic ions in aqueous solutions. The absolute values of hydration energies of tetraalkylammonium ions and protonated aliphatic amines monotonically decrease as the chain length of alkyl groups grows.[3,4,6,7,12]

An important example of biological applications of tetraalkylammonium ions is related to their use as molecular probes and blockers of ion channels in biological membranes. The total charge of +1 along with hydrophobic hydrocarbon chains and relatively small dimensions allow tetraalkylammonium ions directly interfere with permeation of K^+ and Na^+ ions through the narrow pores of ion channels and in this way effectively block channel activity. The tetraethylammonium ion, Et_4N^+, is one such widely used blocking agent in membrane channel studies. In particular, extensive studies of potassium ion channel block by Et_4N^+ have shown that it binds directly to the pore from extracellular and intracellular sides.[13–17] In the first computer simulations of Et_4N^+ binding to the KcsA K^+ channel from the external and internal sides[18] two distinctly different modes of binding for D_{2d} and S_4 conformers were predicted. The first mode is described by a partial insertion of the ethyl group of Et_4N^+ (in the S_4 conformation) into the channel selectivity filter and substitution of either an ion or a water molecule in the end positions within the filter pore. In the second binding mode Et_4N^+ binds in D_{2d} conformation to the binding sites at the entrances to the selectivity filter without direct interfering with the permeating ions and/or waters in the selectivity filter. For a better understanding of the underlying differences in these two mechanisms, conclusive data about the conformational properties of the blockers in solution is important. The aim of the present work is therefore to examine tetraalkylammonium ion conformations in water by the joint use of accurate computational chemistry methods and NMR spectroscopy.

2. Methods

Molecular structures and electronic properties of the quaternary ammonium ions (QAIs) Me_4N^+, Et_4N^+, *n*-Pr_4N^+,

 DOI: 10.1039/b203526j

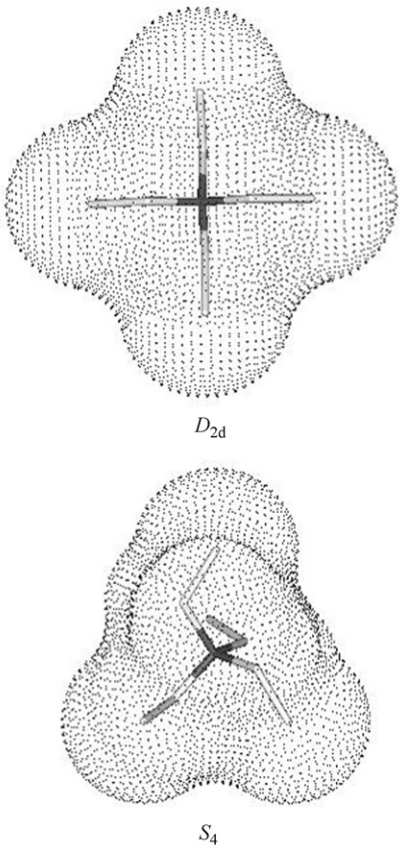

Fig. 1 Structures and molecular surfaces for the D_{2d} and S_4 conformations of Et_4N^+ (atoms H are not displayed).

n-Bu_4N^+, *n*-Pe_4N^+ and the ammonium ion H_4N^+ are calculated with full geometry optimization by means of Hartree–Fock (HF) and density functional theory (DFT) methods (using the Gaussian-98 program[19]) together with several standard Pople-style basis sets. Hydration energies and electronic charge distributions for the ions in aqueous medium are evaluated using the PCM solvent model[20] in Gaussian-98 and the gas-phase optimized structures. Subsequent molecular dynamics (MD) simulations in water employ partial atomic charges that are obtained from the PCM/HF/6-31G(d)//HF/6-31G(d) wave function using the restrained electrostatic potential (RESP) fitting procedure.[21] The RESP procedure involves a two-step conformational averaging of atomic charges where in the first step only the charges on the central N atoms are set equal to each other for the D_{2d} and S_4 conformers, while charges on all C and H atoms are varied independently. In the second step a complete symmetry of charges on the equivalent atoms in the alkyl groups is enforced.

Relative free energies of QAIs in water solution are obtained from microscopic free energy perturbation (FEP) MD calculations. Calculations of relative free energies follow the conventional FEP protocol (see, *e.g.*, discussions given elsewhere[22,23]), where the potential surfaces of initial and final states of the model system are 'connected' *via* a set of intermediate mapping potentials. The free energy associated with the transformation from the potential ε_i to ε_j in n discrete steps is obtained as a sum over the averages $\langle\ \rangle_m$ evaluated on the corresponding potential surfaces ε_m

$$\Delta G(i \rightarrow j) = \Delta G(\vec{\lambda}_0 \rightarrow \vec{\lambda}_n) = -RT \sum_{m=0}^{m=n-1} \ln\langle \exp[-(\varepsilon_{m'} - \varepsilon_m)/RT] \rangle_m,$$
$$\varepsilon_m = \lambda_1^m \varepsilon_i + \lambda_2^m \varepsilon_j \qquad (1)$$

The mapping vector $\vec{\lambda}_m = (\lambda_1^m, \lambda_2^m)$ changes between the values (1,0) and (0,1) for the initial and final states, respectively, with the constraint $\lambda_1^m + \lambda_2^m = 1$. In the FEP calculations 50–60 ps have been given for system equilibration and 159 ps for the system mutation. Typically 53 values of $\vec{\lambda}_m$ are taken in the range between (1,0) and (0,1) and interspaced for optimal sampling efficiency. The calculation at each value of $\vec{\lambda}_m$ included 0.5 ps of initial equilibration and 2.5 ps for data collection, from which the free energies are calculated from the forward run using eqn. (1). Convergence errors in the trajectory sampling are estimated comparing FEP results from several different MD trajectories.

The MD calculations are carried out with the united atom Gromos-87/SPC and all-atom Amber-95/TIP3P force fields (FFs) for ammonium ions and water molecules using the program Q.[24] The RESP PCM/HF/6-31G(d) atomic charges for solutes are used in both FFs, where in Gromos-87 charges on the united C atoms incorporate charges of the attached H atoms. The model systems consist of an ammonium ion surrounded by a 25.0 Å radius sphere of water molecules (*ca.* 2100 waters). In the MD simulations the solute N atom is restrained to the centre of the sphere. Long-range electrostatic interactions are treated by a multipole expansion beyond 10 Å, following the local reaction field method.[25] Spherical water boundary conditions are employed according to the SCAAS model.[24,26] The solvent bond lengths are constrained to their values using the conventional SHAKE procedure. In the FEP calculations MD trajectories with and without SHAKE constraints for the solute bond lengths are examined. The FEP/MD trajectories are calculated at a constant temperature of 300 K and a time step of 2 fs.

The NMR experiments were performed over the temperature range of 278 K–353 K using a 500 MHz (Bruker DRX-500) spectrometer with $\delta_{CH_3CN} = 2.00$ ppm as internal reference in D_2O, with 64 K data points and 32 scans. The selective homonuclear ^1H decoupling experiments have been performed with decoupling power of 50 dB.

3. Results and discussion

3.1. Conformational and solution properties of quaternary ammonium ions from quantum mechanical calculations

Equilibrium geometrical parameters of QAIs show fairly small changes upon the theory level. For example the N–H bond length in H_4N^+ is 1.0137 Å at the HF/6-31G(d) level and 1.0260 Å from the B3LYP/6-311+G(2d,p) geometry optimizations. Similarly, in Me_4N^+ the N–C and C–H bond lengths are 1.4959 Å and 1.0794 Å from HF/6-31G(d) and 1.5057 Å and 1.0877 Å from B3LYP/6-311+G(2d,p) calculations, respectively. However, the dependence of electronic charge distribution upon the theory level is much larger. The largest changes are in atomic charges derived from Mulliken population analysis (MPA). For example, the net charge on atom N in H_4N^+ changes from −1.064 for HF/6-31G(d) to −0.432 for the HF/6-311+G(2d,p) calculations (Table 1). Similarly large variations of the MPA derived atomic charges are found for other ions (Tables 1 and 2), and in general there is no monotonic change in their values with respect to the theory level. Electrostatic potential (ESP) derived partial atomic charges, especially the ESP charges from the PCM calculations where the solute-solvent polarization is taken into account, show much lower dependence on the theory level (Tables 1 and 2). For the considered ions ESP charges on the central N atom are in most cases greater than MPA charges. The ESP HF/6-31G(d) atomic charges (the least computationally expensive) are quite similar to the corresponding atomic charges from higher levels of theory. Unfortunately, the ESP atomic charges show a fairly large conformational dependence that,

Table 1 Partial charges on atom N in H_4N^+ and Me_4N^+ derived from Mulliken population analysis (MPA) and electrostatic potential (ESP) fit[a]

	H_4N^+				Me_4N^+			
	Gas		Water		Gas		Water	
Basis set	MPA	ESP	MPA	ESP	MPA	ESP	MPA	ESP
HF/6-31G(d)	−1.064	−0.866	−0.972	−0.881	−0.559	0.268	−0.552	0.353
HF/6-31G(d,p)	−0.658	−0.886	−0.674	−0.905	−0.588	0.212	−0.581	0.322
HF/6-31+G(d)	−0.951	−0.859	−1.107	−0.890	−0.701	0.253	−0.594	0.391
HF/6-31+G(d,p)	−0.700	−0.882	−0.736	−0.906	−0.459	0.215	−0.354	0.362
HF/6-311+G(2d,p)	−0.432	−0.854	−0.474	−0.881	−0.503	0.171	−0.354	0.351
B3LYP/6-31G(d,p)	−0.587	−0.790	−0.602	−0.808	−0.393	0.209	−0.387	0.325
B3LYP/6-31+G(d)	−1.014	−0.803	−1.061	−0.827	−0.835	0.206	−0.717	0.361
B3LYP/6-31+G(d,p)	−0.698	−0.804	−0.738	−0.828	−0.605	0.148	−0.491	0.310
B3LYP/6-311+G(2d,p)	−0.401	−0.798	−0.444	−0.825	−0.480	0.155	−0.309	0.349

[a] Charges are calculated using the gas-phase HF/6-31G(d) optimized structures.

for example, can be clearly seen by comparing the data for the D_{2d} and S_4 conformations of Et_4N^+ (Table 2). This deficiency is largely removed by using the conformationally averaged atomic charges from the RESP fitting procedure. For heavy atoms, which are hidden inside the molecule and are not well defined in the ESP fitting procedure, charges are hyperbolically restrained to zero values in the RESP method. Such a restraining procedure produces a less polarized charge distribution and improves the description of solute electrostatics compared to straightforward using of MPA derived atomic charges.[21] The RESP partial atomic charges for selected QAIs calculated using the PCM/HF/6-31G(d)//HF/6-31G(d) model are shown in Fig. 2. It is noteworthy that the absolute values of the RESP charges on the central atom N are much smaller compared to the corresponding MPA derived atomic charges, and approximately one half of the total cation charge in the RESP calculations is distributed over four methylene groups adjacent to the central N atom (Fig. 2).

The Et_4N^+ ion can adopt several conformations corresponding to different molecular shape. The quasi-pyramidal S_4 and quasi-planar D_{2d} structures of Et_4N^+ are the low-energy symmetric conformers separated by higher energy intermediates. *GG*1 and *GG*2 are two such intermediate conformations obtained from D_{2d} and S_4 by rotation of one or two ethyl groups (Fig. 3). The D_{2d} and S_4 structures are energetically favourable due to the absence of destabilizing g^+g^- non-bonded interactions between the end methyl groups, while in *GG*1 and *GG*2 two methyl groups are involved in such interactions. Calculated energies for the Et_4N^+ conformers are given in Table 3. In the gas phase the D_{2d} conformation is predicted to be the most stable one. For S_4 the relative gas-phase total electronic energy, ΔE_{el}, is 0.81 kcal mol^{-1} from the HF/6-31G(d) treatment, and 0.87 kcal mol^{-1} from the B3LYP/6-31G(d,p) calculations. Further extension of theory level up to B3LYP/6-311+G(d,p)//B3LYP/6-311+G(d,p) provides a similar value for this energy gap, 0.97 kcal mol^{-1}. Addition of thermal corrections at both HF and DFT levels slightly increases the energy difference between D_{2d} and the other conformers (Table 3). However, the relative stability of D_{2d} goes down, when effects of the polarizable polar environment are taken into account. The corresponding relative free energies in solution, ΔG_{aq}, for the D_{2d} and S_4 conformations are 0.74 and 0.91 kcal mol^{-1} at the HF/6-31G(d) and the B3LYP/6-31G(d,p) levels, respectively. The *GG*1 and *GG*2 conformers are less stable than D_{2d} in the gas phase by 4.1–4.3 kcal mol^{-1} from HF and by 3.8–3.9 kcal mol^{-1} from DFT calculations. Inclusion of solvation energies stabilises these conformers by 0.2–0.4 kcal mol^{-1} relative to D_{2d} (Table 3) Quantum mechanical calculations of larger QAIs (n-Pr_4N^+, n-Bu_4N^+, and n-Pe_4N^+) at the HF/6-31G(d)//HF/6-31G(d) level predict similar to Et_4N^+ conformational energies. In gas phase the energy gap between D_{2d} and S_4 is 0.75 kcal mol^{-1} for n-Pr_4N^+, 0.76 kcal mol^{-1} for n-Bu_4N^+, and 0.77 kcal mol^{-1} for n-Pe_4N^+. In solution the corresponding energy gaps are 0.65 kcal mol^{-1}, −0.15 kcal mol^{-1}, and 0.13 kcal mol^{-1}, respectively (Table 4).

The energy diagram of the Et_4N^+ conformers and the interconnecting torsion barriers calculated at the HF/6-31G(d) level are presented in Fig. 3. Two rotational reaction paths between the D_{2d} and S_4 conformers are considered. The first one presents a two step transition $D_{2d} \rightarrow GG1 \rightarrow S_4$, while the second one includes three steps $D_{2d} \rightarrow GG1 \rightarrow GG2 \rightarrow S_4$. These

Table 2 Partial charges on atom N in Et_4N^+ (D_{2d} and S_4 conformations)[a]

	D_{2d}, Et_4N^+				S_4, Et_4N^+			
	Gas		Water		Gas		Water	
Basis set	MPA	ESP	MPA	ESP	MPA	ESP	MPA	ESP
HF/6-31G(d)	−0.602	−0.288	−0.603	−0.224	−0.599	−0.113	−0.602	−0.052
HF/6-31G(d,p)	−0.624	−0.278	−0.626	−0.211	−0.624	−0.113	−0.626	−0.048
HF/6-31+G(d)	−0.585	−0.280	−0.561	−0.204	−0.567	−0.099	−0.539	−0.024
HF/6-31+G(d,p)	−0.509	−0.277	−0.487	−0.198	−0.473	−0.098	−0.446	−0.021
HF/6-311+G(2d,p)	0.086	−0.293	0.169	−0.157	0.074	−0.120	0.159	−0.007
B3LYP/6-31G(d,p)	−0.406	−0.258	−0.409	−0.189	−0.404	−0.094	−0.407	−0.028
B3LYP/6-31+G(d)	−0.753	−0.284	−0.728	−0.202	−0.778	−0.118	−0.748	−0.040
B3LYP/6-31+G(d,p)	−0.671	−0.292	−0.650	−0.209	−0.684	−0.138	−0.657	−0.058
B3LYP/6-311+G(2d,p)	−0.153	−0.292	−0.065	−0.142	−0.134	−0.119	−0.044	−0.006

[a] Charges are calculated using the gas-phase HF/6-31G(d) optimized structures.

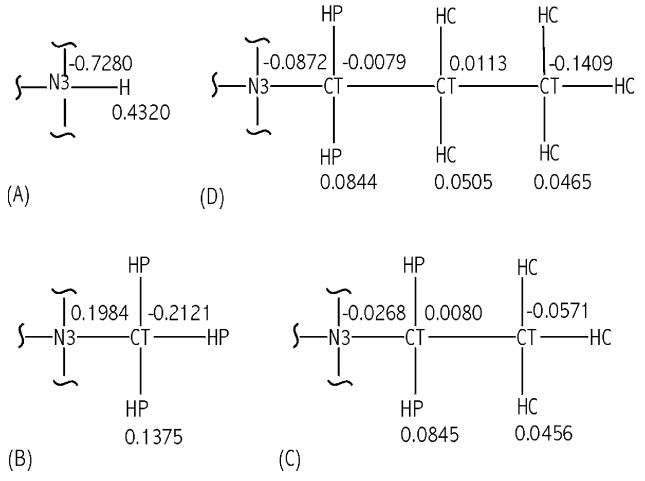

Fig. 2 The calibrated RESP HF/6-31G(d) charges (and Amber-95 atom types) for the selected QAIs. The fragments of H_4N^+ (A), Me_4N^+ (B), Et_4N^+ (C), and *n*-Pr_4N^+ (D) are displayed.

mechanisms are similar to mechanisms for interconversion of the D_{2d} and S_4 conformations of Et_4C.[1] Selected torsion barriers for Et_4N^+ (without considering the two-step mechanism) at the HF/3-21G//HF/STO-3G level have been previously reported elsewhere.[8] In our calculations the barrier for the first step $D_{2d} \rightarrow GG1$, 9.0 kcal mol^{-1}, is very similar to the earlier reported[8] barrier for rotation of a single ethyl group, 8.5 kcal mol^{-1}, in $D_{2d} \rightarrow C_1$ step and is approximately 2 kcal mol^{-1} higher than the barrier in Et_4C from molecular mechanics calculations using MM2 FF. Another intermediate considered elsewhere,[8] C_2, is obtained from rotation of two opposite ethyl groups of the D_{2d} structure and apparently differs from *GG*2, which is obtained from rotation of adjacent ethyl groups in D_{2d}. C_2 has higher energy than *GG*2. The barrier calculated in the present work for the $D_{2d} \rightarrow GG1 \rightarrow GG2 \rightarrow S_4$ mechanism is ~0.8 kcal mol^{-1} lower than the barrier for the three-step mechanism reported elsewhere.[8] The calculated barrier for the $GG1 \rightarrow S_4$ transition is only 5.8 kcal mol^{-1}, which gives approximately 9.5 kcal mol^{-1} for the total barrier of the two-step mechanism in gas-phase. The overall barrier for the three-step mechanism is equal to 12.4 kcal mol^{-1} (Fig. 3). Thus, the two-step mechanism for interconversion of the D_{2d} and S_4 conformations of Et_4N^+ is more favourable than the alternative three-step mechanism. Noteworthy, the energy ranking of the two mechanisms is opposite to what was predicted from molecular mechanics calculations for conformational transitions in Et_4C.[1]

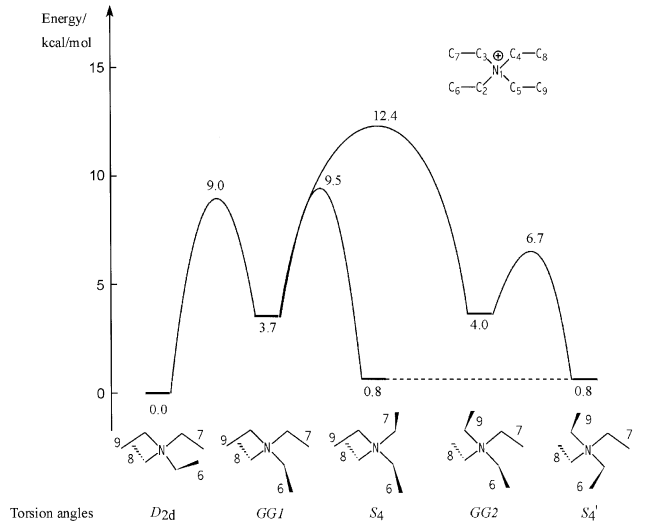

Torsion angles	D_{2d}	*GG1*	S_4	*GG2*	S_4'
(6-2-1-4)	180	34	65	37	-65
(7-3-1-5)	180	176	65	-175	-174
(8-4-1-2)	180	178	174	177	-174
(9-5-1-3)	180	169	174	-66	-65

Fig. 3 Schematic views, relative HF/6-31G(d) energies, and interconnecting torsional barriers for the Et_4N^+ conformations.

Table 3 Relative quantum mechanical energies for the selected Et_4N^+ conformations[a]

Theory level	Energies/ kcal mol^{-1}	Conformation			
		D_{2d}	S_4	*GG*1	*GG*2
HF/6-31G(d)// HF/6-31G(d)	ΔE_{el}	0	0.81	3.69	3.95
	ΔZPVE	0	0.03	0.14	0.07
	ΔG_g	0	0.97	4.26	4.09
	$\Delta\Delta G_{sol}$	0	−0.23	−0.22	−0.43
	ΔG_{aq}	0	0.74	4.04	3.66
B3LYP/6-31G(d,p)// B3LYP/6-31G(d,p)	ΔE_{el}	0	0.87	3.29	3.73
	ΔZPVE	0	0.01	0.06	0.03
	ΔG_g	0	1.11	3.81	3.90
	$\Delta\Delta G_{sol}$	0	−0.20	−0.18	−0.23
	ΔG_{aq}	0	0.91	3.63	3.67

[a] Conformations of Et_4N^+ are displayed in Fig. 1 and 3. Notations for the energies are: ΔE_{el}: total electronic energies in gas phase, ΔZPVE: zero-point vibrational energies, ΔG_g: gas-phase electronic free energies including thermal corrections at 298.15 K, $\Delta\Delta G_{sol}$: hydration free energies from the PCM model, $\Delta G_{aq} = \Delta\Delta G_g + \Delta\Delta G_{sol}$: free energies in water. All values are given relative to D_{2d}. In DFT calculations thermal free energies are corrected for hindered rotations of the end methyl groups.[27] Harmonic vibrational frequencies are scaled by 0.8929 in HF, and by 0.9614 in DFT calculations.

It is also of interest to compare rotation barriers around a single C–N bond in several ammonium ions. Here, we take as a reference rotation barriers in C_2H_5–N^+H_3 and C_2H_5–$N^+(CH_3)_3$. The calculated HF/6-31G(d) rotation barriers in these two molecules are 2.6 kcal mol^{-1} and 5.5 kcal mol^{-1}, respectively. Comparing these values with rotation barriers in Et_4N^+ one can clearly notice the increasing effect of the steric clash between the –Et and other groups (–H, –Me, –Et) at the quaternary centre. Further elongation of the hydrocarbon chains, *i.e.* moving to *n*-Pr, *n*-Bu, and *n*-Pe groups, is

Table 4 Calculated and experimental solvation energies/kcal mol^{-1} of QAIs

Ion	Experiment		Calculations	
	ΔH_{sol}	ΔG_{sol}		ΔG_{sol} (PCM)
H_4N^+	-84.0 ± 3,[12] −88.2[4]	-78 ± 3[12]		−79.88
Me_4N^+	−51.9,[3] −60.0[4]	-51.0 ± 0.5		−52.06
Et_4N^+	−42.1,[3] −57.1[4]	-43.5 ± 0.5[a]	D_{2d}	−43.69
			S_4	−43.92
n-Pr_4N^+	−48.0,[3] -60.0 ± 1[a]	-41.0 ± 1[a]	D_{2d}	−37.20
			S_4	−37.10
n-Bu_4N^+	−62.1[7]	—	D_{2d}	−33.18
			S_4	−34.08
n-Pe_4N^+	—	—	D_{2d}	−31.36
			S_4	−31.98

[a] Extrapolated values based on the data given elsewhere.[3,4,7,12] Experimental values of ΔH_{sol} are based on the $\Delta H_{sol}^{\circ}(H^+) = -271.5$ kcal mol^{-1} as discussed elsewhere.[7] The ΔH_{sol} for *n*-Pr_4N^+ is interpolated using the values for Et_4N^+[4] and *n*-Bu_4N^+.[7] Single point quantum mechanical PCM calculations are performed at the HF/6-31G(d) theory level using the gas-phase HF/6–31G(d) optimized structures.

not expected to introduce changes in g^+g^- interactions at the quaternary centre compared to Et_4N^+. However, possible rotations around the C–C bonds make the potential surface for transitions between D_{2d} and S_4 conformers in the ions with long hydrocarbon chains more complex (see, *e.g.*, discussion elsewhere[1]).

Experimental results and calculated PCM values for the absolute solvation free energies, ΔG_{sol}, of QAIs are given in Table 4. Direct experimental values of ΔG_{sol} for quaternary ammonium ions other than H_4N^+ are unfortunately not available. However, these can be reliably evaluated from the extensive data on solvation thermodynamics of the protonated aliphatic amines.[12] Besides, two sets of solvation enthalpies, ΔH_{sol}, for tetraalkylammonium ions have been reported.[3,4,7] Thermodynamics data[12] provides explicit entropies of solvation for protonated amines with hydrocarbon chains of varying length. Following that we estimate the $T\Delta S$ terms for Me_4N^+, Et_4N^+, and *n*-Pr_4N^+ equal 9.0 kcal mol^{-1}, 13.5 kcal mol^{-1}, 18.0 kcal mol^{-1}, respectively. Using these values and the recent values[4,7] of ΔH_{sol}, we obtain ΔG_{sol} for the selected ions (Table 4). The calculated values of ΔG_{sol} agree reasonably well with the experimental estimates for Me_4N^+ and Et_4N^+. As for *n*-Pr_4N^+, the PCM calculations predict that ΔG_{sol} in this case is 6–7 kcal mol^{-1} greater than for Et_4N^+, while the experimental estimates and the FEP/MD method predict a smaller value for this difference. The decrease in the slope of ΔG_{sol} upon incremental elongation of hydrocarbon groups apparently comes from counterbalancing effects of the enthalpy and entropy contributions. The insufficiently accurate ΔG_{sol} for larger ions from the PCM calculations might be explained by underestimating the hydrophobic effect in this model. However, the PCM method still predicts successively smaller changes in ΔG_{sol} upon going from *n*-Pr_4N^+ to *n*-Bu_4N^+ and to *n*-Pe_4N^+.

3.2. FEP/MD calculations of the relative hydration energies of Et_4N^+ and Pr_4N^+ conformations

Modern microscopic statistical mechanical simulation methods based on molecular mechanics FFs for the solute and water molecules provide an accurate way of evaluating solvation thermodynamics. Here, we calculate the relative solvation free energies of QAIs using the FEP/MD approach (eqn. (1)) where 'non-chemical' transformations (mutation) of ion structures to each other, A → B, are performed. The relative solvation energies, $\Delta\Delta G_{sol}$, are calculated after subtracting gas-phase mutation energy in the related thermodynamic cycle

$$\Delta\Delta G_{sol}(A \rightarrow B) = \Delta G(A \rightarrow B)_{solvent} - \Delta G(A \rightarrow B)_{gas} \quad (2)$$

Two successive transformations of QAIs are examined, namely *n*-$Pr_4N^+ \rightarrow Et_4N^+$ and $Et_4N^+ \rightarrow Me_4N^+$. In view of the relatively high barriers between the D_{2d} and S_4 conformations of tetraalkylammonium ions, MD simulations (on the typical time-scale of nanoseconds) of these ions will essentially sample trajectories only for a single conformer that is given by the initial solute structure. Therefore, the FEP transformations allow for an estimate of the relative free energies of D_{2d} and S_4 conformers in solution. In principle, such conformational energies could be directly calculated by evaluating the potential of mean force (PMF) for the conformational transition in solution. However, the necessity of considering multiple torsion angles and multiple rotational pathways that are involved in $D_{2d} \leftrightarrow S_4$ transitions makes the pmf study of tetraalkylammonium ion conformers presumably more involved than the alternative FEP approach, which provides a straightforward (although indirect) estimate of their relative conformational solvation energies.

The FEP mutations of QAI structures involve gradual changing of atom types, C → H and H → d, in molecular topology and the corresponding FFs. The latter atomic transformation describes annihilation and creation of atoms H in the specified positions and involves dummy atoms (d) with zero values of non-bonded parameters. Transformations of QAI structures are performed only in one direction ('shrinking' of the molecule) in order to produce 'mutation paths' just for the single pre-selected conformation at the quaternary centre. The 'single topology' approach is employed in each case. The H–d bond length is shortened by a factor of 0.55 compared to C–H bond length in order to avoid sampling problems at the end points of transformations. Solute atomic point charges and bond lengths are calibrated from the results of *ab initio* calculations (Fig. 2). The N3–CT bond length is changed from the original Amber-95 value of 1.471 Å to 1.496 Å in Me_4N^+, and 1.517 Å in Et_4N^+ and *n*-Pr_4N^+. Solvation energies from FEP simulations should also include a PMF correction for the changes in bond lengths when the SHAKE procedure is used. However, in calculations of the relative solvation energies for conformations of the same molecule (see Table 5) the PMF contribution cancels out to a good approximation.

The relative solvation energies for the alchemical transformations that involve conformers of Me_4N^+, Et_4N^+, and *n*-Pr_4N^+ are given in Table 5. In case of using the SHAKE constraints the relative solvation free energies for the $Et_4N^+ \rightarrow Me_4N^+$ mutation typically fall into the range from −4 to −5 kcal mol^{-1}. This value comes very close to the experimental difference of −7.5 kcal mol^{-1} after adding the pmf correction, which equals from −2.7 to −3.2 kcal mol^{-1} for the considered molecular transformations.[6,28] The changes of $\Delta\Delta G_{sol}$ for the *n*-$Pr_4N^+ \rightarrow Et_4N^+$ transformation using SHAKE are in the range from −0.1 to +0.7 kcal mol^{-1}, which again approaches the experimental estimate from Table 4 after adding the PMF correction. The calculated free energy differences in the case of not using the SHAKE procedure are close to what is obtained from simulations using SHAKE constraints and the PMF corrections. However, sampling of the FEP/MD trajectories without SHAKE constraints on the solute bond lengths gives somewhat larger fluctuations than sampling of the trajectories of the same time duration where the SHAKE constraints are applied. Such a problem can be in fact expected since using SHAKE constraints technically just helps to avoid unproductive sampling of solute bond-stretching contributions. The calculated values of $\Delta\Delta\Delta G_{sol}$ using the PCM and the FEP/MD simulations with two molecular mechanics FFs (Table 5) show that the S_4 conformation of Et_4N^+ is slightly better solvated

Table 5 Relative solvation free energies (kcal mol^{-1}) for the D_{2d} and S_4 conformations of Et_4N^+ and *n*-Pr_4N^+ from FEP/MD and PCM methods[a]

	$\Delta\Delta\Delta G_{sol}$		
Ion transformation	FEP/ Amber-95	FEP/ Gromos-87	QM/PCM
$(Et_4N^+ \rightarrow Me_4N^+)_{D_{2d}-S_4}$	0.0 (−0.3)	−0.4 (−0.1)	−0.23
$(n\text{-}Pr_4N^+ \rightarrow Et_4N^+)_{D_{2d}-S_4}$	0.4 (0.0)	0.8 (0.5)	0.33

[a] Differences of solvation free energies between two conformers for mutations $A \rightarrow B$ are estimated as $\Delta\Delta\Delta G_{sol}(A \rightarrow B)_{D_{2d}-S_4} = (\Delta G_{sol}(B) - \Delta G_{sol}(A))_{D_{2d}} - (\Delta G_{sol}(B) - \Delta G_{sol}(A))_{S_4}$. Note, that for the $Et_4N^+ \rightarrow Me_4N^+$ transformation this expression reduces to the solvation free energy difference between the D_{2d} and S_4 conformers of Et_4N^+, $\Delta\Delta\Delta G_{sol}(Et_4N^+ \rightarrow Me_4N^+)_{D_{2d}-S_4} \equiv \Delta G_{sol}(Et_4N^+)_{S_4} - \Delta G_{sol}(Et_4N^+)_{D_{2d}}$. The FEP/MD results are provided both with and without SHAKE constraints for the solute bond lengths, where the former values are given in the brackets. The solvation free energies $\Delta\Delta G_{sol}$ for each transformation are calculated as averages from FEP/MD runs over 6 trajectories with different equilibration times (50–100 ps) with a typical error bar of 0.3 kcal mol^{-1}. Single point PCM calculations are performed at the HF/6-31G(d) theory level.

than the D_{2d} structure by up to -0.4 kcal mol^{-1}. For *n*-Pr_4N^+ the estimated difference of solvation energies between the S_4 and D_{2d} conformers is from 0.0 kcal mol^{-1} to $+0.8$ kcal mol^{-1} from the FEP/MD simulations, and $+0.1$ kcal mol^{-1} from the PCM calculations (using data in Table 4).

The solvation free energy difference between two low-energy conformers Et_4N^+ was recently estimated[29] as -0.9 kcal mol^{-1} (in favour of D_{2d}) using another type of FEP/MD procedure. This value differs by more than 1 kcal mol^{-1} from the results of our quantum mechanical and FEP/MD simulations. In the mentioned calculations[29] the $\Delta\Delta G_{sol}$ contains only the electrostatic contribution, which was estimated by gradually switching solute atomic charges to zero values while keeping all other structural parameters unchanged. In principle this type of computational procedure may be considered less accurate than ours, since it does not take into account the possible difference in van der Waals solute-solvent interactions for the two conformers. Using of the overpolarized MPA derived atomic charges for TEA[29] may also partially explain the deviation from the results of our calculations based on the RESP charges. As a consequence, the noted simulations[29] predict a substantially overestimated (see below) value, 1.8 kcal mol^{-1}, for the total free energy difference between the D_{2d} and S_4 conformations of Et_4N^+.

3.3. NMR study of Et_4N^+ in aqueous solution

Fig. 4 shows the ^{1}H NMR spectra of Et_4N^+–I^- in water solution. When considering the Et_4N^+ NMR spectra it is instructive to remember the corresponding data for amines. The nitrogen lone pair in ethylamine lies either *cis* or *trans* to the methyl group,[30] where the quadrupolar $^3J(^{14}N–H)$ coupling is dependent on both the torsional angle $\Phi_{N–C–C–H}$ and the nitrogen lone pair orientation. The functional dependence of $^3J(^{14}N–H)$ on $\Phi_{N–C–C–H}$ for both *cis* or *trans* conformations shows[30] that $^3J(^{14}N–H)$ varies from 2–3 Hz for both conformations at $\Phi_{N–C–C–H} \approx 0°$. As the angle $\Phi_{N–C–C–H}$ approaches 90°, $^3J(^{14}N–H)$ for both *cis* or *trans* conformations comes close to zero. For the *cis* conformation, the $^3J(^{14}N–H)$ value approaches 6–7 Hz when the angle $\Phi_{N–C–C–H} \approx 180°$, whereas the *trans* conformation at this torsion angle shows a coupling constant of $\approx$1 Hz. However, such an influence of the nitrogen lone pair on the preferred rotation to eclipsed (*cis*) and staggered (*trans*) conformations disappears in tetra-*N*-alkylammonium ions.

For Et_4N^+, $^3J_{CH_2–CH_3}$ remains approximately constant ($\sim$7.3 Hz) over the temperature range of 278–353 K. All methylene (Panels (AI)–(AIII) in Fig. 4) and methyl protons (Panels (BI)–(BIII) in Fig. 4) are isochronous over this temperature range, which shows that all four ethyl groups around the nitrogen are chemically and magnetically equivalent on the NMR time scale in aqueous solution. Such equivalence of ethyl groups is supported also by considering the $^3J(^{14}N–H)$ quadrupolar coupling. Fig. 4 indicates that each resonance of the 1 : 2 : 1 triplet pattern of $–CH_3$ is split further to a 1 : 1 : 1 triplet due to the $^3J(^{14}N–H)$ coupling. However, this $–CH_3$ resonance disappears to a singlet (still with 1 : 1 : 1 triplet structure due to $^3J(^{14}N–H)$) on ^{1}H decoupling of $–CH_2$ at 278 K and 353 K (Panels (DI) and (DIII) in Fig. 4). As reported earlier[31] the $^2J(^{14}N–H)$ value is comparatively small (<0.2–0.3 Hz), which is difficult to detect, since the isochronous $–CH_2$ gives a broad singlet upon ^{1}H decoupling of $–CH_3$ (Panel (CI) in Fig. 4). The observed equivalence of ethyl groups can be due to either the presence of a single symmetric structure of Et_4N^+, or averaging of signals for two or more symmetric conformers. Results of the present theoretical calculations as well as of recent Raman spectroscopy studies[10] clearly indicate the presence of two stable conformations of Et_4N^+ in water. This makes the second of the above alternatives the most probable. However, since we do not see any

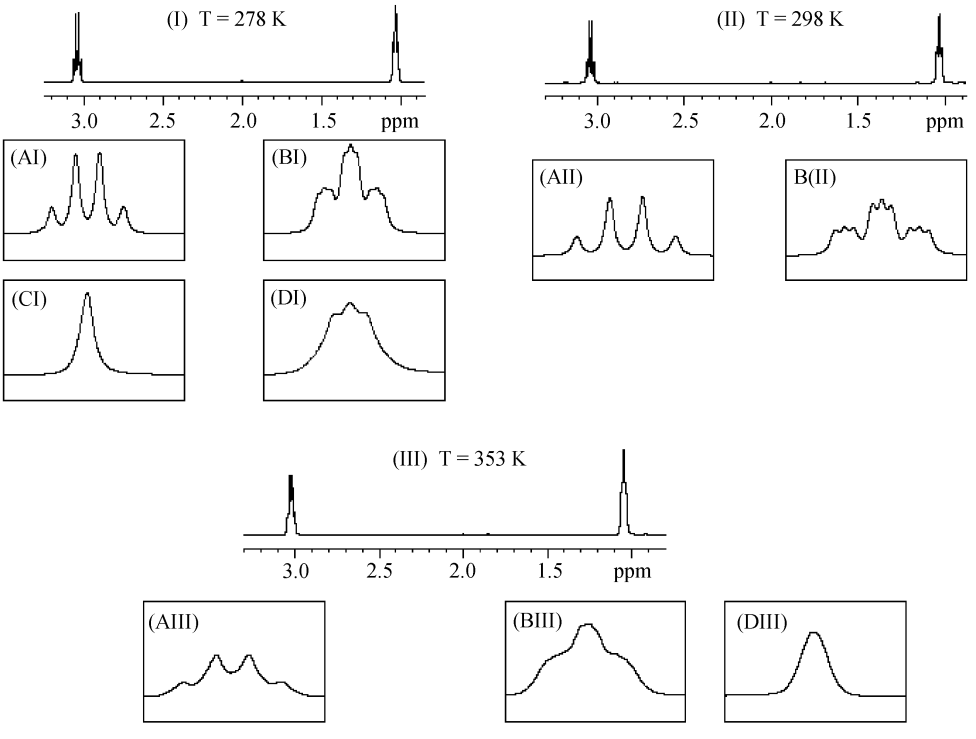

Fig. 4 The ^{1}H NMR spectra for Et_4N^+ iodide in D_2O at 278 K (Panel (I)), 298 K (Panel (II)) and 353 K (Panel (III)). Panels (AI), (AII) and (AIII) show the expanded spectral region for methylene ($\delta_{CH_2} \sim 1.03$ ppm, quartet) resonances and Panels (BI), (BII) and (BIII) show the expanded spectral region for methyl ($\delta_{CH3} \sim 3.03$ ppm, triplet with each further splitted to a 1 : 1 : 1 triplet due to ^3J ($^{14}N–H$) quadrupolar coupling) resonances at 278 K, 298 K and 353 K respectively. Panels (CI) and (DI) show the ^{1}H homodecoupling spectra for the δ_{CH_2} resonances (with decoupling of δ_{CH_3}) and for the δ_{CH_3} resonances (with decoupling of δ_{CH_2}) respectively at 278 K. Panels (DIII) shows the ^{1}H homodecoupling spectra for the δ_{CH_2} resonances (with decoupling of δ_{CH_3}) at 353 K.

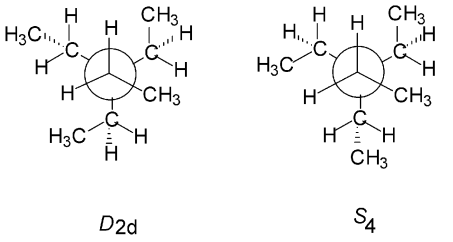

Fig. 5 Newman projections along C–N bond for the D_{2d} and S_4 conformations of Et_4N^+, where indistinguishable methylenes do not allow clear identification of the NMR spectra for the conformers.

change of linewidth in the temperature range of *ca.* 65°, it can be concluded that the D_{2d} and S_4 conformations of are indistinguishable in the recorded NMR spectra. Such spectral similarity of D_{2d} and S_4 is supported on a qualitative level from considering the corresponding Newman projections (Fig. 5), which show that positions of methylene protons in these conformers differ just by permutation and otherwise are equivalent. The previously reported ^{13}C NMR studies of QAIs clarified the structure of Et_4N^+ in complexes with zeolites[8] and mobility of long hydrocarbon chains,[32] but did not address the conformational equilibrium in solution. On the other hand, the indistinguishable character of the D_{2d} and S_4 conformations in ^1H NMR was noted for Et_4C, as well.[1]

4. Conclusions

The NMR study of the Et_4N^+ iodide salt predicts a symmetric structure for this ion in aqueous solution. The exact assignment of the observed spectra to one of two possible symmetric conformations, D_{2d} or S_4, is, however, not possible, since both are expected to give very similar patterns of proton couplings. Quantum mechanical calculations show that the S_4 conformation of Et_4N^+ has a higher gas-phase free energy than the D_{2d} by typically 1.0–1.1 kcal mol^{-1}. D_{2d} interconverts to S_4 *via* a two-step mechanism with an energy barrier of 9.5 kcal mol^{-1}. Such barrier is 3.5 kcal mol^{-1} lower than the previously predicted value for a three-step interconversion mechanism[8] and, in principle, allows fairly rapid transitions between the two rotational isomers. The conformational equilibrium between D_{2d} and S_4 of Et_4N^+ in solution is indeed observed in the Raman spectroscopy studies[10] at room temperatures. Calculations of hydration free energies using QM/PCM and FEP/MD methods predict that the S_4 conformation of Et_4N^+ is better solvated than D_{2d} by approximately −0.2 kcal mol^{-1}. Thus, theoretical calculations predict a free energy difference on the order of RT between the two stable conformations of Et_4N^+. The predicted value closely agrees with the 1.0 kcal mol^{-1} energy gap between the D_{2d} and S_4 conformations of Et_4N^+ in solution estimated from the temperature dependence of their Raman spectra.[10] For the S_4 and D_{2d} conformers of *n*-Pr_4N^+, *n*-Bu_4N^+, and *n*-Pe_4N^+ computational results predict a less than 1.0 kcal mol^{-1} energy difference similarly to Et_4N^+.

The crystal structure of the Et_4N^+ iodide salt shows the S_4 conformation,[2,5] while in the crystallographic study of the Et_4N^+ bromide salt the D_{2d} conformation is observed.[9] The recent database analysis[1] had shown that the S_4 and D_{2d} conformers of Et_4N^+ are observed in the ratio of 45 : 163 (0.28) in 208 different molecular complexes. It is of interest to note that such a ratio well agrees with the theoretical estimate 0.44 for the relative population of the D_{2d} and S_4 conformers in solution from our calculations. The latter value is obtained using the corresponding DFT gas-phase free energy difference, the FEP/MD average estimate of the free energy gap (Tables 3 and 5) and the multiplicity ratio 3 : 6 for D_{2d} and S_4. It is also noteworthy that in host–guest complexes in zeolites Et_4N^+ adopts one of the high-energy conformations characterised by unfavourable g^+g^- interactions.[8] The database analysis for 35 *n*-Pr_4N^+ complexes shows that the two conformations are met in the ratio of 13:22.[1] Finally, if one considers QAIs with even longer hydrocarbon chains it is important to mention the crystallographic complex of the KcsA potassium ion channel with a heavy atom analogue of *n*-Bu_4N^+.[33] In this example the quaternary ion is modelled in a high-energy *gg*-type conformation, although the resolution does apparently not give full details of the ion structure. Thus, the bulk of the structural results indicate that QAIs (including Et_4N^+) can adopt either D_{2d} or S_4 conformation in molecular complexes with other molecules. The actual structure of the ion thus appears to be strongly related to its local environment.

Acknowledgements

Support from the Swedish Research Council (VR) is gratefully acknowledged.

References

1 R. W. Alder, P. R. Allen, K. R. Anderson, C. R. Butts, E. Khosravi, A. Martin, C. M. Maunder, A. G. Orpen and C. B. St. Pourçain, *J. Chem. Soc., Perkin Trans. 2*, 1998, 2083, and references therein.
2 E. Wait and H. M. Powell, *J. Chem. Soc.*, 1958, 1872.
3 D. A. Johnson and J. F. Martin, *J. Chem. Soc., Dalton Trans.*, 1973, 1585.
4 Y. Nagano, M. Sakiyama, T. Fujiwara and Y. Kondo, *J. Phys. Chem.*, 1988, **92**, 5823.
5 B. R. Vincent, O. Knop, A. Linden, T. S. Cameron and K. N. Robertson, *Can. J. Chem.*, 1988, **66**, 3060.
6 B. G. Rao and U. C. Singh, *J. Am. Chem. Soc.*, 1989, **111**, 3125.
7 Y. Nagano, H. Mizuno, M. Sakiyama, T. Fujiwara and Y. Kondo, *J. Phys. Chem.*, 1991, **95**, 2536.
8 H. V. Brand, L. A. Curtiss, L. E. Iton, F. R. Trouw and T. O. Brun, *J. Phys. Chem.*, 1994, **98**, 1293, and references therein.
9 M. Ralle, J. C. Bryan, A. Habenschuss and B. Wunderlich, *Acta Crystallogr., Sect. C.*, 1997, **C53**, 488, and references therein.
10 C. Naudin, F. Bonhomme, J. L. Bruneel, L. Ducasse, J. Grondin, J. C. Lassègues and L. Servant, *J. Raman Spectrosc.*, 2000, **31**, 979, and references therein.
11 E. L. Eliel, S. H. Wilen, and L. N. Mander, *Stereochemistry of Organic Compounds*, Wiley, New York, 1994.
12 D. H. Aue, H. M. Webb and M. T. Bowers, *J. Am. Chem. Soc.*, 1974, **98**, 318.
13 B. Hille, *J. Gen. Physiol.*, 1967, **50**, 1287, and references therein.
14 C. M. Armstrong, *J. Gen. Physiol.*, 1971, **58**, 413, and references therein.
15 B. Hille, *Ionic Channels of Excitable Membranes*, Sinauer Associates, Sunderland, MA, 2nd edn., 1992.
16 L. Heginbotham and R. MacKinnon, *Neuron*, 1992, **8**, 483.
17 D. del Camino, M. Holmgren, Y. Liu and G. Yellen, *Nature*, 2000, **403**, 321, and references therein.
18 V. B. Luzhkov and J. Åqvist, *FEBS Lett.*, 2001, **495**, 191, and references therein.
19 M. J. Frisch, G. W. Trucks, H. B. Schlegel, G. E. Scuseria, M. A. Robb, J. R. Cheeseman, V. G. Zakrzewski, J. A. Montgomery, Jr., R. E. Stratmann, J. C. Burant, S. Dapprich, J. M. Millam, A. D. Daniels, K. N. Kudin, M. C. Strain, O. Farkas, J. Tomasi, V. Barone, M. Cossi, R. Cammi, B. Mennucci, C. Pomelli, C. Adamo, S. Clifford, J. Ochterski, G. A. Petersson, P. Y. Ayala, Q. Cui, K. Morokuma, D. K. Malick, A. D. Rabuck, K. Raghavachari, J. B. Foresman, J. Cioslowski, J. V. Ortiz, A. G. Baboul, B. B. Stefanov, G. Liu, A. Liashenko, P. Piskorz, I. Komaromi, R. Gomperts, R. L. Martin, D. J. Fox, T. Keith, M. A. Al-Laham, C. Y. Peng, A. Nanayakkara, C. Gonzalez, M. Challacombe, P. M. W. Gill, B. G. Johnson, W. Chen, M. W. Wong, J. L. Andres, M. Head-Gordon, E. S. Replogle and J. A. Pople, *Gaussian 98 (Revision A.1)*, Gaussian, Inc., Pittsburgh PA, 1998.
20 M. Cossi and V. Barone, *J. Chem. Phys.*, 1998, **109**, 6246.

21 C. I. Bayly, P. Cieplak, W. D. Cornell and P. Kollman, *J. Phys. Chem.*, 1993, **97**, 10 269.
22 W. F. van Gunsteren and H. J. C. Berendsen, *Angew. Chem., Int. Ed. Engl.*, 1990, **29**, 992.
23 P. Kollman, *Chem. Rev.*, 1993, **93**, 2395, and references therein.
24 J. Marelius, K. Kolmodin, I. Feierberg and J. Åqvist, *J. Mol. Graph. Modell.*, 1999, **16**, 213, and references therein.
25 F. S. Lee and A. Warshel, *J. Chem. Phys.*, 1992, **97**, 3100.
26 G. King and A. Warshel, *J. Chem. Phys.*, 1989, **91**, 3647.
27 K. S. Pitzer and W. D. Gwinn, *J. Chem. Phys.*, 1942, **10**, 428.
28 D. A. Pearlman and P. Kollman, *J. Chem. Phys.*, 1991, **94**, 4532.
29 S. Crouzy, S. Bernèche and B. Roux, *J. Gen. Physiol.*, 2001, **118**, 207.
30 R. Wasylishen, in *Nuclear Magnetic Resonance Spectroscopy of Nuclei Other Than Protons*, ed. T. Axenrod, and G. A. Webb, John Wiley & Sons, Inc., 1981, p. 105.
31 K. Tori, T. Iwata, K. Aono, M. Ohtsuru and T. Nakagawa, *Chem. Pharm. Bull.*, 1967, **15**(3), 329, and references therein.
32 F. Coletta, A. Ferrarini, F. Gottardi and P. L. Nordio, *Chem. Phys.*, 1995, **192**, 19.
33 M. Zhou, J. H. Morais-Cabral, S. Mann and R. MacKinon, *Nature*, 2001, **411**, 657.